

Raman scattering study of magnetic layered MPS_3 crystals (M=Mn, Fe, Ni)

Yi-Meng Wang(王艺朦), Jian-Feng Zhang(张建丰), Cheng-He Li(李承贺), Xiao-Li Ma(马肖莉), Jian-Ting Ji(籍建葶), Feng Jin(金峰), He-Chang Lei(雷和畅), Kai Liu(刘凯), Wei-Lu Zhang(张玮璐), Qing-Ming Zhang(张清明)

Citation: Chin. Phys. B . 2019, 28(5): 056301. **doi:** 10.1088/1674-1056/28/5/056301
Journal homepage: http://cpb.iphy.ac.cn; http://iopscience.iop.org/cpb

What follows is a list of articles you may be interested in

Simulation and experimental investigation of low-frequency vibration reduction of honeycomb phononic crystals

Han-Bo Shao(邵瀚波), Guo-Ping Chen(陈国平), Huan He(何欢), Jin-Hui Jiang(姜金辉)

Chin. Phys. B . 2018, 27(12): 126301. **doi:** 10.1088/1674-1056/27/12/126301

Magnetism and piezoelectricity of hexagonal boron nitride with triangular vacancy

Lu-Si Zhao(赵路丝), Chun-Ping Chen(陈春平), Lin-Lin Liu(刘林林), Hong-Xia Yu(于洪侠), Yi Chen(陈怡), Xiao-Chun Wang(王晓春)

Chin. Phys. B . 2018, 27(1): 016301. **doi:** 10.1088/1674-1056/27/1/016301

Raman phonons in multiferroic $FeVO_4$ crystals

Zhang An-Min, Liu Kai, Ji Jian-Ting, He Chang-Zhen, Tian Yong, Jin Feng, Zhang Qing-Ming

Chin. Phys. B . 2015, 24(12): 126301. **doi:** 10.1088/1674-1056/24/12/126301

Effect of Gd doping on the magnetism and work function of $Fe_{1-x}Gd_x$/Fe (001)

Tang Ke-Qin, Zhong Ke-Hua, Cheng Yan-Ming, Huang Zhi-Gao

Chin. Phys. B . 2014, 23(5): 056301. **doi:** 10.1088/1674-1056/23/5/056301

Effect of 6H-SiC (1120) substrate on epitaxial graphene revealed by Raman scattering

Lin Jing-Jing, Guo Li-Wei, Jia Yu-Ping, Chen Lian-Lian, Lu Wei, Huang Jiao, Chen Xiao-Long

Chin. Phys. B . 2013, 22(1): 016301. **doi:** 10.1088/1674-1056/22/1/016301

Raman scattering study of magnetic layered MPS_3 crystals (M = Mn, Fe, Ni)*

Yi-Meng Wang(王艺朦)[1], Jian-Feng Zhang(张建丰)[1], Cheng-He Li(李承贺)[1], Xiao-Li Ma(马肖莉)[2], Jian-Ting Ji(籍建葶)[2], Feng Jin(金峰)[1], He-Chang Lei(雷和畅)[1], Kai Liu(刘凯)[1], Wei-Lu Zhang(张玮璐)[3], and Qing-Ming Zhang(张清明)[2,4,†]

[1] *Department of Physics, Renmin University of China, Beijing* 100872, *China*
[2] *Beijing National Laboratory for Condensed Matter Physics, Institute of Physics, Chinese Academy of Sciences, Beijing* 100190, *China*
[3] *Department of Engineering and Applied Sciences, Sophia University,* 7-1 *Kioi-cho, Chiyoda-ku, Tokyo* 102-8554, *Japan*
[4] *School of Physical Science and Technology, Lanzhou University, Lanzhou* 730000, *China*

(Received 12 February 2019; revised manuscript received 16 March 2019; published online 8 April 2019)

We report a comprehensive Raman scattering study on layered MPS_3 (M = Mn, Fe, Ni), a two-dimensional magnetic compound with weak van der Waals interlayer coupling. The observed Raman phonon modes have been well assigned by the combination of first-principles calculations and the polarization-resolved spectra. Careful symmetry analysis on the angle-dependent spectra demonstrates that the crystal symmetry is strictly described by C_{2h} but can be simplified to D_{3d} with good accuracy. Interestingly, the three compounds share exactly the same lattice structure but show distinct magnetic structures. This provides us with a unique opportunity to study the effect of different magnetic orders on lattice dynamics in MPS_3. Our results reveal that the in-plane Néel antiferromagnetic (AF) order in $MnPS_3$ favors a spin–phonon coupling compared to the in-plane zig-zag AF in $NiPS_3$ and $FePS_3$. We have discussed the mechanism in terms of the folding of magnetic Brillouin zones. Our results provide insights into the relation between lattice dynamics and magnetism in the layered MPX_3 (M = transition metal, X = S, Se) family and shed light on the magnetism of monolayer MPX_3 materials.

Keywords: Raman scattering, two-dimensional magnetic van der Waals materials, lattice dynamics, magnetism

PACS: 63.20.–e, 63.22.–m, 75.75.–c, 78.30.–j **DOI:** 10.1088/1674-1056/28/5/056301

1. Introduction

One of the current research interests in two-dimensional (2D) materials focuses on magnetic van der Waals (vdW) materials, due to the intriguing physical properties for both fundamental research and potential applications in optoelectronics, spintronics, and valleytronics. A number of potentially magnetic single-layer vdW materials have recently been proposed, including V-based dichalcogenides, $CrGeTe_3$ ternary tritellurides, and CrX_3 trihalides. Studies on CrI_3 reveal that it has a stable ferromagnetic (FM) ordering in 2D form and a little change of layer-number dependence of Curie temperatures.[1–5] This has attracted a lot of attention in other magnetic vdW crystals that are similar to CrI_3.[6–12]

Recently, many studies have focused on the magnetic van der Waals crystals MPX_3, which resemble similar lattice structure and chemical composition.[13–16] MPX_3 is a family of 2D vdW layered crystals that have been prepared and studied for two decades. The structure of bulk MPS_3 is similar to CrI_3 which adopts the monoclinic $AlCl_3$ structure (point group C_{2h}). The layer structure is anchored by $(P_2X_6)^{4-}$ bipyramids in a triangular lattice which provide enclosures for transition metal (TM) atoms arranged in a hexagonal array.[17–23] The monolayer MPS_3 has a perfect honeycomb lattice similar to graphene. For magnetism in MPS_3, the intralayer magnetic structures are antiferromagnetic (AF). However, depending on the variety of TM atoms, magnetic structures possess very rich types. For $MnPS_3$ material, the AF phase transition temperature T_N is 78 K. The magnetic moment is 3.5 μ_B[23] and the spin lies in the ab plane with inclined angle. The magnetic structure of $MnPS_3$ in the ab plane is Néel AF in which the spin of the two adjacent magnetic ions is reversed and the magnetism along the c-axis is FM ordering. For $FePS_3$, its T_N is 120 K and the spin moment is along the c-axis. In the ab plane, the magnetic structure is zigzag-type AF ordering in which the two adjacent magnetic ions are the same and are opposite to the third neighbor. Along the c-axis, the magnetic order is AF type. For $NiPS_3$, its T_N is 150 K and the angle between the spin and the c-axis is less than 30°. The intralayer magnetic structure of $NiPS_3$ is zigzag-type which is the same as $FePS_3$, while the interlayer magnetic order is FM type.[10]

Raman is a useful tool to study the structure and magnetic properties of ultrathin vdW single crystals. Meanwhile, there are several spectroscopic studies in $FePS_3$ and $NiPS_3$. In the previous studies of thin layer $FePS_3$ and $NiPS_3$, two different point groups, C_{2h} and D_{3d}, have been proposed when

*Project supported by the Ministry of Science and Technology of China (Grant Nos. 2016YFA0300504 and 2017YFA0302904), the National Natural Science Foundation of China (Grant Nos. 11474357 and 11774419), the Fundamental Research Funds for the Central Universities, China, and the Research Funds of Renmin University of China (Grant No. 14XNLQ03).

†Corresponding author. E-mail: qmzhang@ruc.edu.cn

© 2019 Chinese Physical Society and IOP Publishing Ltd

discussing the phonon modes and the lattice structure.[13,14] However, no consensus has yet been reached. The information on $MnPS_3$ is still lacking. A comparative study of the phonon spectra in MPS_3 (M = Mn, Fe, Ni) is important for the clarification of this issue. Moreover, the temperature dependence behaviors of magnetism in MPS_3 have not been studied or discussed in detail. Therefore, this calls for a systematic research of the phonon spectra and magnetic properties in MPS_3 materials with different transition metals.

In this paper, we present temperature-dependent and polarization-resolved Raman spectroscopy study on layered MPS_3 (M = Mn, Fe, Ni) single crystals. Almost all of the Raman active phonons are observed, and the phonon mode assignments are made by symmetry analysis and comparison with first principle calculations. In particular, we conduct a comparative study of Raman spectra in $MnPS_3$, $FePS_3$, and $NiPS_3$, which share identical lattice structure but exhibit distinct magnetic order, and their temperature evolution crosses the magnetic transition. Consequently, we provide comprehensive information on the relation of the lattice dynamics and magnetism in the MPS_3 system.

2. Experimental and calculation methods

Single crystals of MPS_3 (M = Mn, Fe, Ni) were grown by chemical vapor transport (CVT) method. The crystal naturally cleaves along the (001) surface, forming $MnPS_3$ flakes weakly bonded by van der Waals force. In this experiment, the $MnPS_3$ flakes were cleaved from bulk single crystals, transferred on to silicon substrates, and capped with 90 nm silicon oxide (SiO_2) because of the transparent characteristic. The SiO_2 capping layer does not induce any extra signal in the energy range we are interested in and can enhance Raman scattering signal intensity from the sample. The $FePS_3$ and $NiPS_3$ single crystals were tested on the copper holder directly. The temperature-dependent and polarization-resolved Raman spectra were collected in a backscattering configuration using an HR800 spectrometer (Jobin Yvon) equipped with a liquid-nitrogen-cooled charge-coupled device (CCD) and volume Bragg gratings. The samples were placed in an ultra high vacuum (UHV) cryostat with a vacuum of $\sim 10^{-8}$ mbar. A $\lambda = 633$ nm laser was focused to a 5×5 μm^2 spot on the ab surface of the sample. The scattered signal was collected through a 50× long focus-length objective, and dispersed with a 600 grooves/mm grating. The laser power was kept at approximately ~ 1.4 mW. We define X and Y axes inside the crystallographic ab plane. X is perpendicular to the b axis and Y is along the b axis. Z is perpendicular to X and Y.

First-principles calculations were employed to work out the Brillouin zone-center (Gamma point) phonon modes of $MnPS_3$. The projector augmented wave (PAW) method implemented in the Vienna *ab initio* simulation package (VASP) package was used to describe core electrons.[24–28] For the exchange–correlation potential, the generalized gradient approximation (GGA) of Perdew–Burke–Ernzerhof formula was adopted.[29] To describe the van der Waals interaction in layered systems not included in the conventional density functional theory, the vdW-optB86b functional was chosen.[30] The on-site Coulomb repulsion among the localized Mn 3d electrons was also included by using the formalism (GGA+U) of Dudarev *et al.*[31] with an effective $U = 5$ eV. The kinetic energy cutoff of the plane-wave basis was set to be 300 eV. The simulations were carried out with a triclinic cell containing two Mn atoms, two P atoms, and six S atoms, in which two Mn atoms took the antiferromagnetic order. An $8\times 8\times 8$ k-point mesh for the Brillouin zone sampling and the Gaussian smearing with a width of 0.05 eV around the Fermi surface were employed. In structure optimization, both cell parameters and internal atomic positions were allowed to relax until all forces were smaller than 0.01 eV/Å. When the equilibrium structure was obtained, the phonon modes at Brillouin zone center were calculated by using the dynamic matrix method. The calculations with a 10-atom cell gave 27 optical modes. However, to illustrate the displacement patterns of phonon modes, we show our results in a 20-atom supercell deduced from the real-space translational invariance of the 10-atom cell; as in Ref. [32].

3. Results and discussion

The MPS_3 crystal has a monoclinic structure with C_{2h} point group (space group $C2/m$). With 10 atoms in a primitive unit cell, we have a total of 30 phonon modes. At the Γ point, there are $8A_g + 7B_g$ Raman active modes. The corresponding Raman tensors are

$$A_g = \begin{pmatrix} b & 0 & d \\ 0 & c & 0 \\ d & 0 & a \end{pmatrix}, \quad B_g = \begin{pmatrix} 0 & f & 0 \\ f & 0 & e \\ 0 & e & 0 \end{pmatrix}.$$

This leads to different angular dependence of the phonon intensity $I(\theta)$ for the A_g and B_g modes in Raman spectra when the incident/scattered light polarizations (e_i/e_s) rotate inside the ab plane

$$e_i \parallel e_s: \begin{cases} A_g: I(\theta) = \left[b\sin^2\theta + c\cos^2\theta\right]^2, \\ B_g: I(\theta) = \left[e\sin(2\theta)\right]^2, \end{cases} \tag{1}$$

$$e_i \perp e_s: \begin{cases} A_g: I(\theta) = \left[\dfrac{(b-c)}{2}\sin(2\theta)\right]^2, \\ B_g: I(\theta) = \left[e\cos(2\theta)\right]^2, \end{cases} \tag{2}$$

where θ is defined as the angle between e_i and the Y axis. From Eqs. (1) and (2), we find that when $\theta = 0$, the A_g phonon only appears under parallel polarization and the B_g phonon only appears under cross polarization; when $\theta = \pi/4$, the A_g phonon appears under both parallel and cross polarizations, while the B_g phonon only appears under parallel polarization.

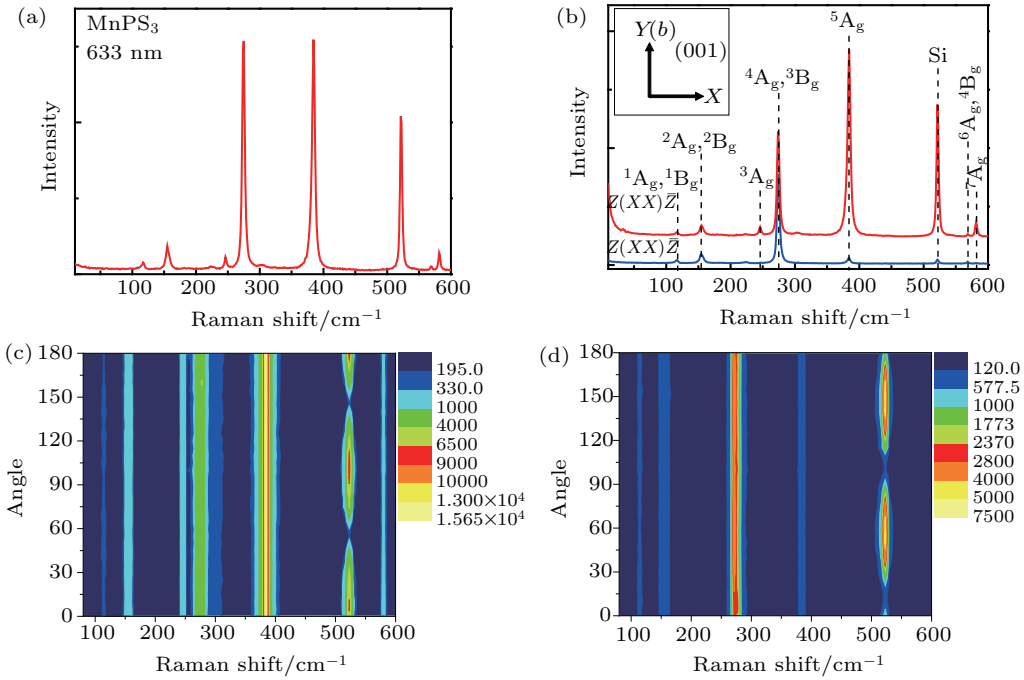


Fig. 1. (a) Unpolarized Raman spectrum of $MnPS_3$ collected at room temperature. (b) Polarized Raman spectra of $MnPS_3$ at room temperature under $Z(XX)\bar{Z}$ (red line) and $Z(XY)\bar{Z}$ (blue line) scattering geometry. Inset: the XYZ/abc coordinates. (c) Intensity map of Raman spectra of $MnPS_3$ under parallel polarization scattering geometry as a function of Raman shift and angle. (d) Same as (c), but under cross polarization geometry.

Table 1. Calculated and experimental optical phonon modes (in cm^{-1}) for $MnPS_3$. The atomic motions of the modes are also given (see Fig. 4). R and IR denote Raman and infrared activities, respectively.

Symmetry	Calculated/cm^{-1}	Experimental/cm^{-1}	Activity
^1B_g	59.7		R
^1A_g	116.5	115.5	R
^2B_g	121.2	115.5	R
^1B_u	147.7		IR
^3B_g	151.1	153.8	R
^2A_g	152.5	153.8	R
^2B_u	154.4		IR
^1A_u	154.8		IR
^2A_u	183.0		IR
^3B_u	190.1		IR
^3A_u	194.0		IR
^4B_g	202.6		R
^5B_g	221.4		R
^3A_g	224.7		R
^4A_g	242.9	245.0	R
^4B_u	244.5		IR
^4A_u	248.0		IR
^6B_g	263.9	270.0	R
^5A_g	266.2	270.0	R
^5B_u	304.0		IR
^6A_g	360.0	383.2	R
^6B_u	425.2		IR
^7A_g	538.8	567.5	R
^7B_g	539.8	567.5	R
^7B_u	539.9		IR
^5A_u	542.2		IR
^8A_g	543.9	580.3	R

In Figs. 1(a) and 1(b), we show Raman spectra of $MnPS_3$ at room temperature. The peak at 520.7 cm^{-1} is from the Si substrate. All the remaining peaks are the phonons of $MnPS_3$. We assign the three $MnPS_3$ phonons that only appear in XX polarization to A_g mode. However, no phonon modes only appear in the XY scattering geometry. In Figs. 1(c) and 1(d), we track the angular dependence of the phonon intensity under parallel and cross polarizations. Surprisingly, we do not observe any mode that reduces to zero intensity at $\theta = \pi/4$.

To find the origin of the remaining four phonon modes, we consider a change of the lattice symmetry in the 2D van der Waals materials. For monolayer $MnPS_3$, the lattice point group is D_{3d}. At the Γ point, there are $3A_{1g} + 5E_g$ Raman active modes. The corresponding Raman tensors are

$$A_{1g} = \begin{pmatrix} b' & 0 & 0 \\ 0 & b' & 0 \\ 0 & 0 & a' \end{pmatrix},$$

$$E_{g(1)} = \begin{pmatrix} c' & 0 & 0 \\ 0 & -c' & d' \\ 0 & d' & 0 \end{pmatrix},$$

$$E_{g(2)} = \begin{pmatrix} 0 & -c' & -d' \\ -c' & 0 & 0 \\ -d' & 0 & 0 \end{pmatrix}.$$

In this case, the $3A_{1g}$ phonons show maximum intensity under XX polarization configuration and zero intensity under XY polarization configuration, while the intensity of the $5E_g$ phonons does not show strong angular dependence.

The bulk crystals consist of ABC-stacked single layer assemblies that are held together by van der Waals forces. Thus, for bulk crystals, the C_3 symmetry along the c axis has broken compared to the monolayer crystals. Because of the symmetry breaking, the E_g mode in D_{3d} symmetry will degenerate into

A_g and B_g modes which have similar energies in C_{2h} symmetry. Based on the discussion above, for $MnPS_3$, the observed phonons are: 115.5 cm^{-1} (^1A_g, ^1B_g), 153.8 cm^{-1} (^2A_g, ^2B_g), 245.0 cm^{-1} (^3A_g), 270.0 cm^{-1} (^4A_g, ^3B_g), 383.2 cm^{-1} (^5A_g), 567.5 cm^{-1} (^6A_g, ^4B_g), and 580.3 cm^{-1} (^7A_g).

To relate the observed modes at certain frequencies to the specific atomic displacements, we conduct the first-principles calculations. The experimental and calculated mode frequencies are summarized in Table 1. The calculated phonon frequencies are in good agreement with the experimental data. In Fig. 2, we show the atomic displacements of all of the Raman active modes.

Using the same analysis method for $MnPS_3$, we determine the phonon modes for $FePS_3$ and $NiPS_3$. As shown in Fig. 3(a), for $FePS_3$, the observed phonons are: 94.9 cm^{-1} (^1A_g, ^1B_g), 156.9 cm^{-1} (^2A_g, ^2B_g), 223.3 cm^{-1} (^3A_g, ^3B_g), 245.8 cm^{-1}(^4A_g), 275.2 cm^{-1} (^5A_g,^4B_g), 380.9 cm^{-1} (^6A_g), and 582.9 cm^{-1} (^7A_g). Near 275.2 cm^{-1}, the peak energies are slightly different under $Z(XX)\bar{Z}$ and $Z(XY)\bar{Z}$ scattering geometry, which suggests that there are two different modes at very close energy. The splitting of the peak is found at low temperatures, indicating that the symmetry of bulk crystals is C_{2h}. The obvious difference between the two channels of $FePS_3$ at room temperature may be due to the different evolution of different phonon peaks with temperature. The $NiPS_3$ Raman spectra are shown in Fig. 4, where the observed phonon modes are: 132.2 cm^{-1} (^1A_g, ^1B_g), 177.4 cm^{-1} (^2A_g, ^2B_g), 234.8 cm^{-1} (^3A_g, ^3B_g), 255.1 cm^{-1} (^4A_g), 280.7 cm^{-1} (^5A_g, ^4B_g), 384.8 cm^{-1} (^6A_g), and 589.2 cm^{-1} (^7A_g). The experimental results of $FePS_3$ and $NiPS_3$ are in good agreement with the theoretical calculations.[6]

In Fig. 5, we show the Raman spectra in MPS_3 (M = Mn, Fe, Ni) at 10 K, T_N, and 300 K. For all of the samples, we observe that the phonon mode ($\sim$ 260 cm^{-1} at 300 K) splits into two peaks at the lowest temperature. We attribute this to the narrowing of the phonon linewidth at low temperature. Moreover, we observe two unusual temperature-dependent behaviors for MPS_3 (M = Mn, Fe, Ni). Firstly, for $FePS_3$, three new phonon modes appear in the magnetic order phase ($T < T_N$), while we do not observe such additional modes in $MnPS_3$ or $NiPS_3$. This different behavior in $FePS_3$ must be related to its special magnetic structure. We attribute this to the AF interlayer magnetic structure in $FePS_3$, which doubles the lattice unit cell if there is a strong spin–lattice coupling,

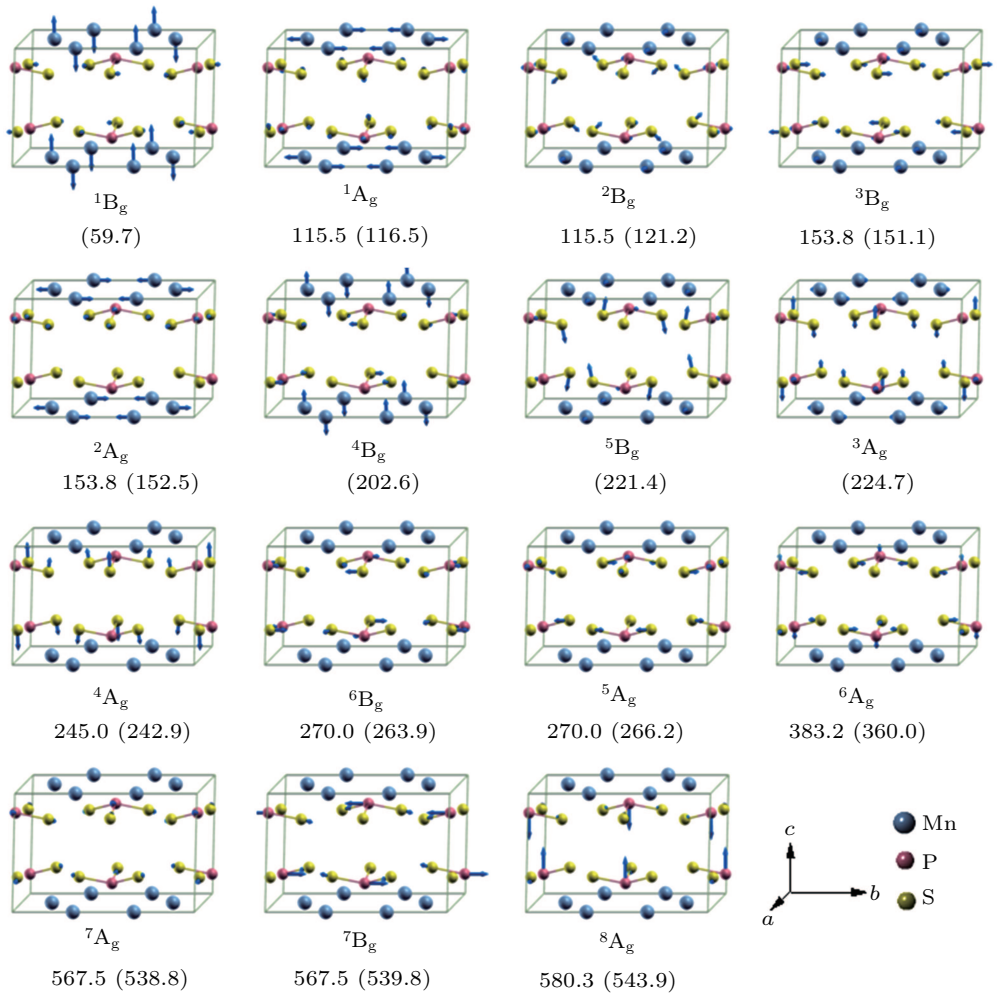


Fig. 2. Vibration patterns of all Raman modes observed in $MnPS_3$. The mode symmetry, optical activity, and experimental (calculated) phonon frequency (the unit is cm^{-1}) are also listed below each pattern.

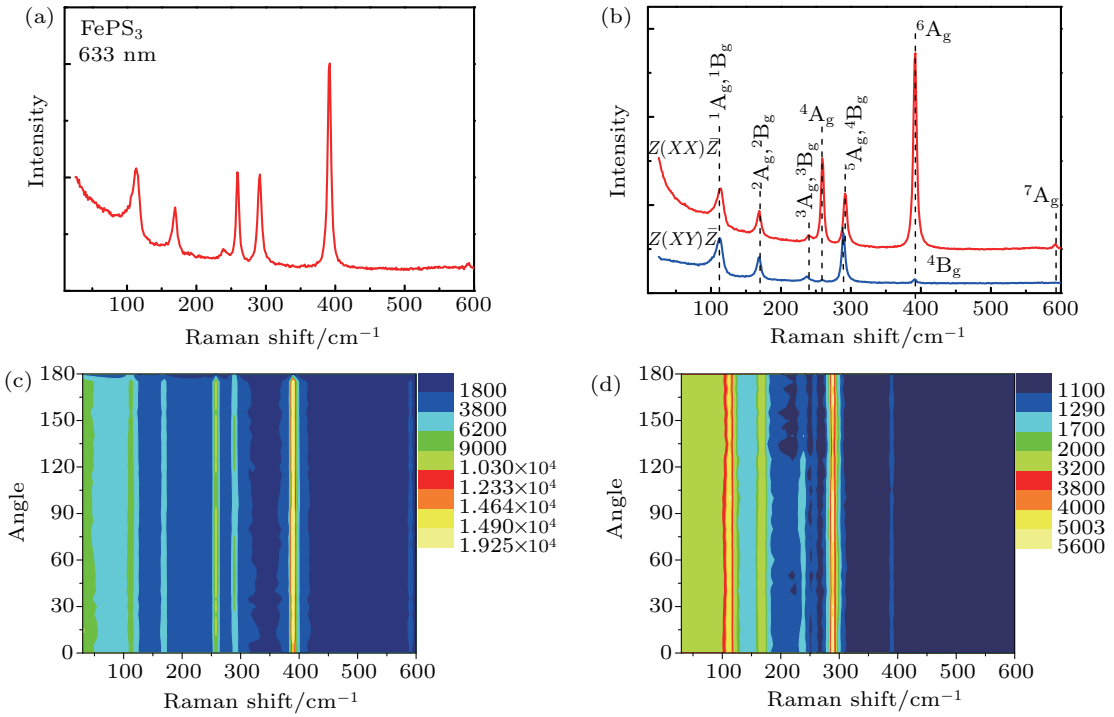


Fig. 3. (a) Raman spectrum of $FePS_3$ collected at room temperature. (b) Polarized Raman spectrum of $FePS_3$ at room temperature under different polarization configurations. (c) The angle-dependent Raman spectrum of $FePS_3$ in parallel polarization channel. (d) The angle-dependent Raman spectrum of $FePS_3$ in cross polarization channel.

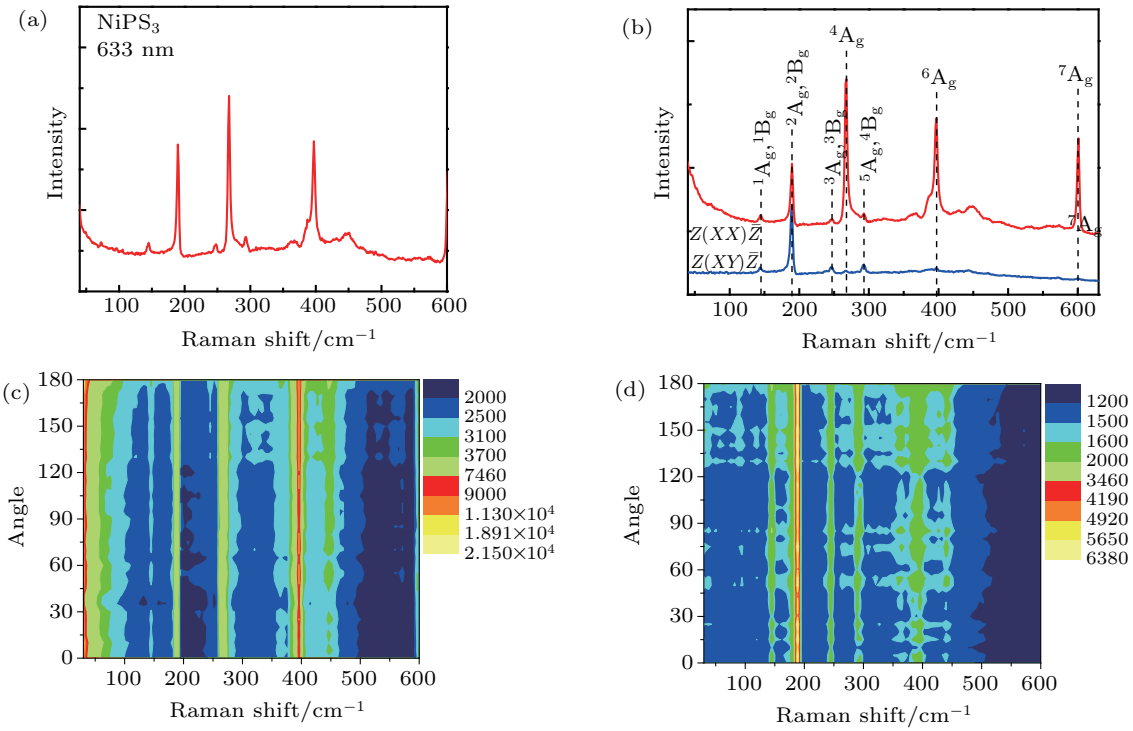


Fig. 4. (a) Unpolarized Raman spectrum of $NiPS_3$ at room temperature. (b) Polarized Raman spectrum of $NiPS_3$ at room temperature under different polarization configurations. (c) The angle-dependent Raman spectrum of $NiPS_3$ in parallel polarization channel. (d) The angle-dependent Raman spectrum of $NiPS_3$ in cross polarization channel.

and, consequently, the zone boundary modes are folded to the Γ point. In Mn/$NiPS_3$, the interlayer magnetic structure is FM, and will not double the lattice unit cell. This explains the non-observation of additional modes in Mn/$NiPS_3$. Secondly, for $MnPS_3$ and $NiPS_3$, they have the same out-of-plane magnetism but different in-plane magnetism. The in-plane magnetism is zig-zag type AF in $NiPS_3$, while the in-plane magnetism is Néel type AF in $MnPS_3$. We find that the energy of the 150 cm^{-1} phonon mode at 10 K is much lower than that at 300 K in $MnPS_3$, which is unusual for a normal phonon mode. The lower energy of this mode at 10 K indicates its coupling with spins, which modulates the self-energy of this

phonon and causes the lower energy of it. This indicates that the in-plane Néel AF in $MnPS_3$ favors a spin–phonon coupling compared to the in-plane zig-zag AF in $NiPS_3$ and $FePS_3$. Comparing the *ab* in-plane and the *c* axis out-of-plane magnetic structure of the series, it is found that spin–phonon coupling is general in this family materials and different magnetic structures will have different influences on the phonons and magnons.

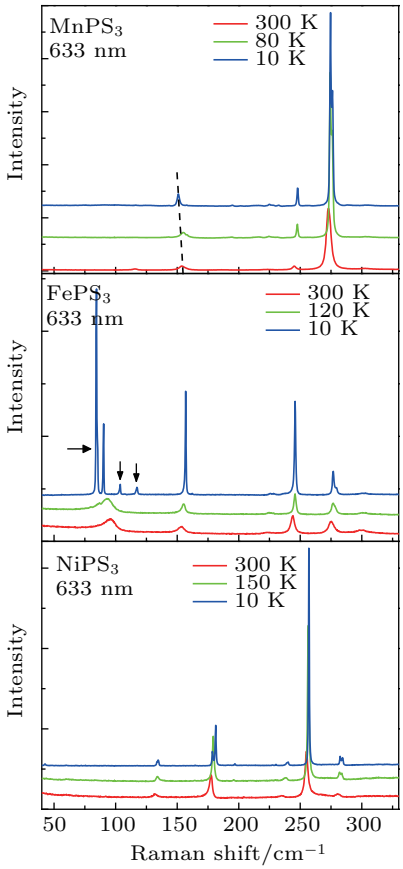


Fig. 5. The temperature dependence of Raman spectra of $MnPS_3$, $FePS_3$, and $NiPS_3$. The dashed line indicates the softened mode in $MnPS_3$ and the arrows indicate the new modes in $FePS_3$ below T_N.

4. Conclusion and perspectives

We report the experimental and first-principles calculation for the temperature dependent and polarization resolved Raman spectroscopy on the lattice dynamics of MPS_3 (M = Mn, Fe, Ni) single crystals. We identify 7 out of 11 Raman active phonons and the corresponding atomic displacements. In addition, we observe additional phonons appearing in $FePS_3$ in the magnetic ordered state, while there is no new phonon mode in $MnPS_3$ and $NiPS_3$. This magneto-elastic effect is related to unique AF order along the *c* axis in $FePS_3$, which doubles the unit cell and folds the zone boundary mode to the Γ point. For $MnPS_3$, part of the phonons are softened below T_N, suggesting spin–phonon coupling in this material. The present study provides the system information on the lattice dynamics and magnetic of MPS_3 (M = Mn, Fe, Ni) and is of significance for the exploration of structural and magnetic properties of the monolayer MPX_3.

Acknowledgments

Computational resources have been provided by the Physical Laboratory of High Performance Computing at Renmin University of China. The atomic structures and vibrational displacement patterns were prepared with the XCRYSDEN program.[33]

References

[1] Huang B, Clark G, Moratalla E N, Klein D R, Cheng R, Seyler K L, Zhong D, Schmidgall E, McGuire M A, Cobden D H, Yao W, Xiao D, Herrero P J and Xu X D 2017 *Nature* **546** 270
[2] Wang H, Fan F, Zhu S and Wu H 2016 *Europhys. Lett.* **114** 47001
[3] Lado J L and Fernández-Rossier J 2017 *2D Mater.* **4** 035002
[4] McGuire M A 2017 *Crystals* **7** 121
[5] Zhong D, Seyler K L, Xia Y, Lin P, Cheng R, Sivadas N, Huang B, Schmidgall E, Taniguchi T, Watanabe K, McGuire M A, Wang Y, Xiao D, Fu C K M and Xu X D 2017 *Sci. Adv.* **3** e1603113
[6] Bernasconi M, Marra G L, Benedek G, Miglio L, Jouanne M, Julien C, Scagliotti M and Balkanski M 1988 *Phys. Rev. B* **38** 12089
[7] Dresselhaus M S 1986 *Intercalation in Layered Materials* (New York: Plenum) p. 93
[8] Chittari B, Park Y, Lee D, Han M, MacDonald A H, Wang E H and Jung J 2016 *Phys. Rev. B* **94** 184428
[9] Du K Z, Wang X Z, Liu Y, Hu P, Utama M I B, Gan C K, Xiong Q and Kloc C 2016 *ACS Nano* **10** 1738
[10] Flem G L, Brec R, Ouvrard G, Louisy A and Segransen P 1982 *J. Phys. Chem. Solids* **43** 455
[11] Joy P A and Vasudevan S 1992 *Phys. Rev. B* **46** 5425
[12] Li X, Cao T, Niu Q, Shi J and Feng J 2013 *Proc. Natl. Acad. Sci.* **110** 3738
[13] Kuo C T, Neumann M, Balamurugan K, Park H J, Kang S, Shiu H W, Kang J H, Hong B H, Han M, Hoh T W and Park J G 2016 *Sci. Rep.* **6** 20904
[14] Lee J U, Lee S, Ryoo J, Kang S, Kim T, Kim P, Park C H, Park J G and Cheong H 2016 *Nano Lett.* **16** 7433
[15] Murayama C, Okabe M, Urushihara D, Asaka T, Fukuda K, Isobe M, Yamamoto K and Matsushita Y 2016 *J. Appl. Phys.* **120** 142114
[16] Wang X Z, Du K Z, Liu Y Y F, Hu P, Zhang J, Zhang Q, Owen M H S, Lu X, Gan C K, Sengupta P, Kloc C and Xiong Q H 2016 *2D Mater.* **3** 031009
[17] Dziaugys A, Banys J and Vysochanskii Y 2013 *Ferroelectrics* **447** 1
[18] Evans J S O, O'Hare D, Clement R, Leaustic A and Thuéry P 1995 *Adv. Mater.* **7** 735
[19] Frindt R F, Yang D and Westreich P 2005 *J. Mater. Res.* **20** 1107
[20] Makimura C, Sekine T, Tanokura Y and Kurosawa K 1993 *J. Phys. Condens. Matter* **5** 623
[21] Piryatinskaya V G, Kachur I S, Slavin V V, Yeremenko A V and Vysochanskii Y M 2012 *Low Temp. Phys.* **38** 870
[22] Wildes A R, Harris M J and Godfrey K W 1998 *J. Magn. Magn. Mater.* **177-181** 143
[23] Wildes A R, Kennedy S J and Hicks T J 1994 *J. Phys. Condens. Matter* **6** L335
[24] Blöchl P E 1994 *Phys. Rev. B* **50** 17953
[25] Kresse G and Joubert D 1999 *Phys. Rev. B* **59** 1758
[26] Kresse G and Hafner J 1993 *Phys. Rev. B* **47** 558
[27] Kresse G and Furthmüller J 1996 *Comp. Mater. Sci.* **6** 15
[28] Kresse G and Furthmüller J 1996 *Phys. Rev. B* **54** 11169
[29] Perdew J P, Burke K and Ernzerhof M 1996 *Phys. Rev. Lett.* **77** 3865
[30] Klimeš J, Bowler D R and Michaelides A 2011 *Phys. Rev. B* **83** 195131
[31] Dudarev S L, Botton G A, Savrasov S Y, Humphreys C J and Sutton A P 1998 *Phys. Rev. B* **57** 1505
[32] Zhang A M, Liu K, He J B, Wang D M, Chen G F, Norm, B and Zhang Q M 2012 *Phys. Rev. B* **86** 134502
[33] Kokalj A 2003 *Comp. Mater. Sci.* **28** 155